

Uncertainty-aware Blood Glucose Prediction from Continuous Glucose Monitoring Data

Hai Siong Tan

Gryphon Center for A.I. and Theoretical Sciences
86 Marine Parade Promenade, Singapore
haisiong.tan@gryphonai.com.sg

Abstract. In this work, we investigate uncertainty-aware neural network models for blood glucose prediction and adverse glycemic event identification in Type 1 diabetes. We consider three families of sequence models based on LSTM, GRU, and Transformer architectures, with uncertainty quantification enabled by either Monte Carlo dropout or through evidential output layers compatible with Deep Evidential Regression. Using the HUPA-UCM diabetes dataset for validation, we find that Transformer-based models equipped with evidential output heads provide the most effective uncertainty-aware framework, achieving consistently higher predictive accuracies and better-calibrated uncertainty estimates whose magnitudes significantly correlate with prediction errors. We further evaluate the clinical risk of each model using the recently proposed Diabetes Technology Society error grid, with risk categories defined by international expert consensus. Our results demonstrate the value of integrating principled uncertainty quantification into real-time machine-learning-based blood glucose prediction systems.

1 Introduction

This work explores machine learning algorithms that generate blood glucose prediction for diabetic patients based on past records of glucose and bolus insulin tracked at regular intervals by Continuous glucose monitoring (CGM) systems, and other physiology-related data. In contrast to the majority of past works in this area [21], here our focus lies in examining the extent to which uncertainty quantification aids in enhancing the effectiveness of the glucose prediction system, the main uncertainty quantification methodologies we examined being Monte Carlo dropout [11] and Deep Evidential Regression [2] techniques. These are incorporated into three families of models based on (i) Long Short-Term Memory (LSTM) [15] (ii) Gated Recurrent Units (GRU) [6] and (iii) Transformer [32] architectures respectively.

We validate our models on the publicly accessible HUPA-UCM dataset of [14] which consists of real clinical data from a medical study of 25 patients with Type 1 diabetes and leverages measurements from CGM devices. As emphasized by a global consensus of diabetes clinicians and technologists in [3, 4, 10], CGM enables real-life tracking of blood glucose levels at a fixed sampling rate and has been established as a powerful method in diabetes management [25]. It can provide time series data suitable for training machine learning models [7, 21] in glucose prediction tasks. Like related recent works in [23, 33], apart from glucose prediction at some fixed-duration horizon (here we chose it to be 30 minutes and 1 hour), we also assessed our models' effectiveness at adverse glycemic event identification — predicting occurrences of hypoglycemia and hyperglycemia. This classification task is of particular importance for Type 1 diabetes patients who require injection of exogenous artificial insulin in the absence of natural insulin secretion [1]. While hyperglycemia is associated with short-term complications like ketoacidosis, acute hypoglycemia can lead to severe convulsions and coma [1, 13], apart from being a major impediment to diabetes therapy intensification [26]. Against the backdrop of potentially severe health consequences in adverse glycemic events, we would like our machine learning models to be reliable in the sense of being equipped with robust uncertainty quantification. Developing effective uncertainty-aware glucose prediction models that leverage CGM data is thus a natural goal towards realizing AI technology that can be used in a reliable way to manage diabetes conditions on a daily basis.

Another theme that characterizes our work here is the use of evaluation metrics that are more clinically motivated. Specifically, in assessing the model's accuracy, we use an error grid published recently by the Diabetes Technology Society (DTS) in November 2024 [18] to evaluate the proportion of model predictions lying in what diabetes clinicians agreed upon as a 'no-risk' region or, in the technical language of [18] — the 'zone A accuracy'. Mathematically, this refers to a thin region surrounding the diagonal in the prediction-ground truth plane that clinicians define as practically the set of glucose values for which model accuracy is enough for safe clinical decision-making. In previous work on machine learning-guided

glucose prediction (e.g. [23, 31, 33]), an older error grid formulated in 1987 known as the Clarke error grid [8] was also used, yet to our knowledge, our work is the first that leverages the most recently updated error grid in [18] for assessing machine learning-based glucose prediction. Another accuracy related metric that, to our knowledge, has been used rather sparingly as compared to say the root-mean-squared-error is the mean absolute relative difference (MARD) which was indicated in the consensus statements of [3, 10] to be the most established metric in measuring the reliability of CGM systems. Here in our context, we take the CGM-measured values as the reference ground truth and leverage MARD for assessing model accuracy. As described in [18], MARD correlates with DTS error grid’s zone A accuracy. We hope that our use of these evaluation metrics (which embody the diabetes clinicians’ expert knowledge to some extent) enables model results to be interpreted in a more clinically meaningful way.

2 Background ideas and related work

In this Section, we discuss several background topics that will enable a clearer understanding of our methodology. As evidential regression is less commonly used in uncertainty quantification compared to the more conventional Monte Carlo dropout technique [11], and we have also used a relatively novel regularizer first proposed in [29] (in a different context), here we furnish a detailed explanation on how to incorporate evidential regression of [2] into various time-series models. Comments on the HUPA-UCM dataset and related literature are also included in this Section.

2.1 Incorporating Deep Evidential Regression into neural network models

In the following, we explain the operational principles of Deep Evidential Regression [2, 27] and how we incorporate it as an uncertainty quantification technique into our models.

Let $\mathcal{M}(z)$ denote the base neural network with z being its input. Here we consider the architectures of long short-term memory (LSTM), gated recurrent units (GRU) and Transformers for $\mathcal{M}(z)$. The uncertainty estimates for each output neuron can be obtained as follows. We first consider a probabilistic model where each output neuron is accompanied by another one representing its uncertainty. This pair of neurons can be interpreted as the Gaussian mean and variance for the probabilistic target. We further assume prior distributions for the mean μ and variance σ^2 and integrate (μ, σ^2) out to obtain a marginal distribution that depends on the observed data and the parameters of the prior distribution. Specifically taking the prior to be a normal-inverse-gamma distribution (NIG) with $\mu \sim \mathcal{N}(\gamma, \sigma^2/\nu)$, $\sigma^2 \sim \Gamma^{-1}(\alpha, \beta)$, we obtain the marginal distribution to be a t-distribution as follows.

$$\begin{aligned} & \iint d\mu d\sigma^2 f_{\mathcal{N}}(y_{obs}; \mu, \sigma^2) f_{NIG}(\mu, \sigma^2; \alpha, \beta, \nu, \gamma) \\ &= \frac{\Gamma(\alpha + \frac{1}{2})}{\Gamma(\alpha) \sqrt{2\pi\beta(1+\nu)/\nu}} \left(1 + \frac{(y_{obs} - \gamma)^2}{2\beta(1+\nu)/\nu}\right)^{-(\alpha + \frac{1}{2})}, \end{aligned} \quad (1)$$

where $f_{\mathcal{N}}$ denotes the auxiliary Gaussian distribution, f_{NIG} the NIG prior and y_{obs} the observed data. Instead of just a single output neuron or a pair representing (μ, σ^2) , the model $\mathcal{M}(z)$ now has four output neurons $(\alpha, \beta, \nu, \gamma)$ where γ represents the mean and α, β, ν are related to the predictive variance σ_p^2 as follows.

$$\sigma_a^2 = \mathbb{E}(\sigma^2) = \frac{\beta}{\alpha - 1}, \quad \sigma_e^2 = \text{Var}(\mu) = \frac{\beta}{(\alpha - 1)\nu}, \quad \sigma_p^2 = \sigma_a^2 + \sigma_e^2, \quad (2)$$

where σ_a^2, σ_e^2 denote the aleatoric and epistemic uncertainties respectively. σ_a^2 is typically interpreted as the uncertainty related to measurement noise while σ_e^2 represents the uncertainty due to data insufficiency and the underlying model’s capacity to represent the observed knowledge [17]. The model $\mathcal{M}(z)$ yields predictions together with the overall uncertainty expressed by σ_p^2 (which is the variance of the t-distribution in eqn. 1) provided it is trained upon a loss function consistent with eqn. (1). Following [2], we take the negative log-likelihood of eqn. (1) as a generalized data loss term \mathcal{L}_{data}

$$\mathcal{L}_{data} = -\log \left[\frac{\Gamma(\alpha + \frac{1}{2}) \left(1 + \frac{(y_{obs} - \gamma)^2}{2\beta(1+\nu)/\nu}\right)^{-(\alpha + \frac{1}{2})}}{\Gamma(\alpha) \sqrt{2\pi\beta(1+\nu)/\nu}} \right]. \quad (3)$$

This replaces the usual mean-squared-error loss term, with the original output layer expanded to a tuple of 4 neurons representing $\{\alpha, \beta, \nu, \gamma\}$ per target variable.

For our glucose prediction models, the inputs z are multivariate physiological signals over a sliding window of some fixed period. In this work, we take the inputs to consist of four-feature sequences over a sliding window of 3 hours. The data is sampled at 5 minutes interval so the input sequence is of length 36. Symbolically,

$$z_t = (x_{t-35}, \dots, x_t) \in \mathbb{R}^{36 \times 4}. \quad (4)$$

The model $\mathcal{M}(z)$ predicts the future glucose trajectory over some fixed horizon h_L . Denoting the set of predicted glucose by \hat{y} ,

$$\hat{y} = (g_{t+1}, \dots, g_{t+h_L}) \in \mathbb{R}^{h_L}, \quad (5)$$

where g_t denotes the predicted glucose level at time t . In our work, we consider two specific values of $h_L = \{6, 12\}$ representing a 30 minutes and 1 hour forecast horizon respectively.¹ Minimally incorporating evidential regression within the model translates to expanding the output layer such that apart from eqn. (5), we have

$$\begin{aligned} \hat{\gamma} &= (g_{t+1}, \dots, g_{t+h_L}), \hat{\alpha} = (\alpha_{t+1}, \dots, \alpha_{t+h_L}) \\ \hat{\beta} &= (\beta_{t+1}, \dots, \beta_{t+h_L}), \hat{\nu} = (\nu_{t+1}, \dots, \nu_{t+h_L}), \end{aligned} \quad (6)$$

where $\hat{\gamma}$ denotes the *mean* glucose level over the prediction horizon, and $\hat{\alpha}, \hat{\beta}, \hat{\nu}$ are the uncertainty-related outputs that can be used following eqn. (2) to construct statistical confidence intervals throughout the prediction horizon. To summarize, the evidential regression models learn a mapping $\mathcal{M} : \mathbb{R}^{36 \times 4} \rightarrow \mathbb{R}^{4 \times h_L}$, where, for each forecast horizon step, the network outputs the four parameters of the evidential predictive distribution.

A subtle aspect of evidential regression lies in the regularization of the learning of uncertainties via augmenting \mathcal{L}_{data} with another loss term designed such that ideally, larger uncertainties are associated with greater prediction errors during model training. In [2], the authors proposed a regularizer constructed to minimize evidence on incorrect predictions that reads $\mathcal{L}_R = |y_{obs} - \gamma|(2\nu + \alpha)$. Although it was claimed in [2] to be reasonable, it is unfortunately independent of β which controls the overall uncertainty scale, as shown in eqn. (2). In [29], the authors proposed a refinement of this original EDL regularizer by multiplying it to the Kullback-Leibler divergence [9, 19] between the distribution described by eqn. (1) and a weakly-informative prior, its final form being (see the Appendix for a detailed derivation)

$$\mathcal{L}_{kl} = |y_{obs} - \gamma| \left(\log \frac{\beta_r^\alpha \Gamma(\alpha)}{\beta^\alpha} + \gamma_e(\alpha - 1) + \frac{\beta - \beta_r}{\beta_r} \right), \quad (7)$$

where γ_e is the Euler-Mascheroni constant. In eqn. (7), β_r is a reference β value which is understood to characterize a weakly informative prior for larger deviations from the observed dataset. We set it to be of the same order-of-magnitude as the maximal value in our glucose dataset. The authors of [29] found this regularizer to perform better than \mathcal{L}_R in the context of Physics-Informed Neural Networks. Theoretically, it aligns with the goal of guiding distributions for erroneous predictions to inherit weak priors with higher uncertainties. To our knowledge, no previous work has considered this information-theoretic regularization term in regression-type contexts.

2.2 On the HUPA-UCM dataset

This is a dataset [14] furnishing real data from a medical study of 25 patients with Type 1 diabetes mellitus (T1DM). It provides CGM data, insulin dose (both bolus volumes and a continuous basal insulin rate) and related physiological quantities: heart rate, steps, calories burned, meal ingestion estimated in carbohydrate grams. CGM data was acquired by FreeStyle Libre 2 systems, while Fitbit Ionic smart watches were used for measuring steps, calories and heart rate data. The sampling rate was five minutes and data for each patient was collected for at least 2 weeks under free-living conditions.

This HUPA-UCM dataset was curated by researchers at the Complutense University of Madrid and Prince of Asturias University Hospital, and made publicly accessible for research purposes without any additional approval procedures required. In our work here, we used the provided preprocessed version of the dataset which required no additional cleaning (e.g. interpolation for missing values, etc.).

¹ These values were also adopted by [33].

2.3 Related Work

We refer the reader to [7, 20, 21] for recent reviews of glucose prediction models in literature, yet we would like to briefly comment on two particular papers which are more intimately connected to our approach.

To our knowledge, the model proposed in [33] was the only prior work in published literature on glucose prediction that examined an uncertainty distribution-equipped model. They had also invoked evidential regression in constructing their model named as ‘Fast-adaptive and Confident Neural Network’, the basic architecture being a stack of 3 bi-directional GRU layers with (128, 64, 32) neurons followed by an attention layer (with 128 neurons) preceding the evidential outputs corresponding to the parameters of the t-distribution. Model training was performed on the OhioT1DM dataset [24] and two other proprietary datasets (of Imperial College London, UK) with roughly a 3:1:1 training/validation/testing chronological split. The loss function is the loss term in eqn. (3) with the regularization term proposed by Amini et al. in [2]. The input sequences were (i)CGM glucose (ii)bolus insulin (iii)carbohydrate intake. Similar to our setup, prediction horizons were taken to be 30 and 60 minutes. However, there were some aspects of uncertainty quantification that were significantly different from our approach: (i)the confidence bands were constructed by taking an empirical parameter representing a ‘z-value’ to the epistemic uncertainty expressed in eqn. (2). In our understanding, this is not quite the correct confidence interval as the predictive variance of the t-distribution is the sum of the aleatoric and epistemic uncertainties, (ii)there was no usage of any metric to assess calibration of uncertainty estimates in [33], (iii)there was no comparison to other uncertainty quantification methods.

In [23], the authors compared LSTM models trained on individual-specific data to those trained on population-level data from the HUPA-UCM dataset. They found that individualized models achieved comparable prediction accuracy to aggregated models, with mean root mean squared error across 25 subjects of 22.52 ± 6.38 mg/dL for the individualized models, 20.50 ± 5.66 mg/dL for the aggregated models, and Clarke error grid Zone A accuracy of $84.07 \pm 6.66\%$ vs. $85.09 \pm 5.34\%$, respectively. Subject-level analyses revealed only modest differences between the two approaches, with some individuals benefiting more from personalized training. The focus in [23] was in examining whether training models on individual-based or population-based data leads to significant differences in results rather than any usage/study of uncertainty quantification techniques. Thus, similar to [33] and other previous works covered in the reviews [7, 21], there was no usage of uncertainty quantification-related metrics. Their choice of input features was one of the four classes that we have used in our work here: { glucose, bolus and basal insulin, carbohydrate intake }.

3 Methodology

3.1 Aspects of model implementation

For each patient, data were split chronologically into 60% training, 20% validation, and 20% testing to avoid temporal leakage. Inputs consist of 4 feature sequences : blood glucose, bolus insulin, carbohydrates intake and one of the following {heart rate, steps, calories, basal insulin}, with all features standardized using z-score normalization. We focus on the prediction horizons $h_L = 30$ min and 1 hour.

Models were trained for 300 epochs using Adam (learning rate 10^{-4} , batch size 1024). Dropout-based models were optimized with mean squared error, whereas evidential models used $\mathcal{L}_{evidential} = \mathcal{L}_{data} + 0.01 * \mathcal{L}_{kl}$ where \mathcal{L}_{data} is defined in eqn. (3) and \mathcal{L}_{kl} defined in eqn. (7). Validation data were used for each model’s hyperparameter selection, and the test set was reserved for final evaluation. All models were trained on an NVIDIA A100 GPU. In the following, we briefly summarize the three neural network base models considered in our experiments and the classical ridge regression baseline method [22].

LSTM This class of models is a unidirectional LSTM that maps the four-dimensional input sequence to a future glucose trajectory. The sequence is processed by a single-layer LSTM with hidden size 128, and the hidden state of the final timestep is used as a compact representation of the historical context. This representation is passed through a fully connected prediction head consisting of a 64-unit linear layer followed by a dropout layer (activated for the model equipped with uncertainty quantification) and a final linear output layer that produces the h_L -step glucose forecast.

GRU We also consider an attentive bidirectional GRU architecture where the input sequence of four-dimensional input sequence is processed by a 3-layer bidirectional GRU with hidden size of 40 per direction, producing temporal representations of dimension 80 at each timestep. A temporal attention mechanism is then applied to the full sequence to compute a weighted context vector summarizing the history, allowing the model to focus on clinically relevant past observations. The resulting context representation is passed through a fully connected prediction head consisting of a 32-unit hidden layer with ReLU activation and a dropout layer, followed by a linear output layer that produces the h_L -step glucose forecast.

Transformers We also consider a causal Transformer encoder where the four-dimensional input sequence is first projected to a model dimension of 64 and augmented with positional encoding. The sequence is then processed by a 2-layer Transformer encoder composed of multi-head self-attention with 4 attention heads and feedforward sub-layers of dimension 128 using GELU activation. A causal attention mask ensures that each timestep attends only to past observations. The hidden representation of the final timestep is used as the sequence summary and passed through a linear output layer to produce the h_L -step glucose forecast.

Ridge Regression As a non-neural network classical baseline, we use Bayesian ridge regression [22]. A Gaussian prior is imposed on the regression weights, and the posterior is computed analytically. Predictions for new input sequences are assumed to be Gaussian distributed, with mean equal to the posterior mean prediction and variance accounting for both residual noise and parameter uncertainty.

3.2 On evaluation of model accuracy

Related literature on blood glucose prediction from CGM datasets often used the Clarke Error Grid [8] as one of the metrics for prediction models. Designed specifically for clinical decision-making, an error grid generally describes the clinical point accuracy of a glucose monitor compared with reference values, with reference/monitor paired values assigned to clinical risk zones. Using such an error grid to assess accuracy of machine-learning-based prediction models enables one to evaluate them in a manner that is more informative with regards to the clinical risks they carry.

An important caveat is that error grids for glucose are based on clinical risk scores determined by diabetes experts reflecting contemporaneous knowledge and evidence. Thus, one anticipates such risk score definitions to evolve over time. Since Clarke Error Grid [8] was developed in 1987, various technological advancements in diabetes care have occurred such as increased usage of new insulin delivery technologies and they have affected expectations that clinicians have for the performance of glucose monitoring devices. To update and enhance appropriateness of error grids for device developers, clinical researchers, regulatory bodies and other professionals working in the field of diabetes management, the Diabetes Technology Society (DTS) convened a panel of 89 international experts in glucose monitoring from 21 countries and developed the DTS Error Grid in [18] as a modern method for rigorous evaluation of accuracy of glucose monitoring devices that takes into account the contemporary clinician input. In the DTS Error Grid, there are five clinical risk zones (A-E) representing { ‘no’, ‘mild’, ‘moderate’, ‘high’, ‘extreme’ } risks respectively. The consensus error grid was described in [3] to be an evaluation tool which can critically shed light whether inaccuracies have effect on clinical decision making. Tables 1 - 6 include the percentage of predictions falling within zone A (no clinical risk) as a representative indicator of the model’s clinical reliability.

Another crucial metric of accuracy that we use is that of the mean absolute relative difference (MARD). As described in an international expert consensus [3, 10], MARD is the most common and established statistic that can be employed to assess the accuracy of CGM devices with respect to corresponding values of some reference system. Here we use it as a measure of model accuracy with respect to the measurements of the CGM device. A larger percentage indicates model predictions deviating further away from the measured values.

3.3 Metrics for assessing uncertainty quantification

To assess uncertainty quantification, we use several metrics : (i) Brier scores, (ii) Spearman’s correlation between uncertainty estimates and prediction errors ($\equiv \rho$), (iii) Spearman’s correlation between uncertainty estimates and the DTS clinical risk zones ($\equiv \rho_z$), and (iv) reliability diagrams plotting empirical

coverage probabilities (ECP) against nominal ones, and the mean calibration error (MCE) defined as the mean absolute value of the deviation between ECP and nominal probabilities.

The adverse glycemic events of primary interest to clinical diabetes management are [3, 10]: hypoglycemia (defined as glucose level < 70 mg/dL) and hyperglycemia (defined as glucose level > 180 mg/dL). The Brier score is defined as the following average [5] $\equiv \frac{1}{N} \sum_{i=1}^N (g_i - y_i)^2$, where g_i, y_i are the model probabilities and observed occurrences for these events respectively, and N refers to the total number of testing data points. This proper scoring rule evaluates the entire predicted probability distribution. For each model, we report sensitivity and precision for hypo- and hyperglycemia detection but these metrics depend on a classification threshold and exhibit a precision–recall trade-off. For probabilistic models, we also evaluate the Brier score for each event, which complements these measures by providing a threshold-independent assessment of probabilistic accuracy.

The couple of Spearman’s coefficients ρ, ρ_z enables us to quantify the degree to which the uncertainty estimates correlate with predictive errors and clinical risks as defined by the consensus of human experts in [18]. We represent the uncertainty estimates by the standard deviation of the uncertainty’s probability distribution. In the case of evidential regression-based models, this is σ_p as defined in eqn. 2. For dropout models, this is the empirical standard deviation of the Monte-Carlo samples, whereas for ridge regression, we used the known analytical formula for the standard deviation of the assumed underlying Gaussian distribution. In particular, ρ_z connects the model’s uncertainty quantification to the diabetes physicians’ knowledge encoded in the risk stratification scheme of [18]. Non-trivial correlations would then suggest that the model’s uncertainty estimates reflect clinically relevant notions of reliability. To compute ρ_z , we represent each DTS clinical risk zone as an ordinal integer from 1 - 5 pertaining to risk zones A - E respectively. ρ_z is then the ordinary Spearman’s coefficient between the uncertainty estimates and the DTS clinical risk zone associated with each model prediction.

Another metric that we use to assess uncertainty quantification is through the empirical coverage probability. For each nominal coverage level $1 - \alpha$, we compute the two-sided predictive intervals using the learned t-distribution in the case of evidential models or empirical quantiles of the samples for dropout-based model. The empirical coverage probability is simply defined as the fraction of observed glucose values contained within the interval. Calibration is assessed by plotting empirical versus nominal coverage and summarized by the mean absolute coverage error, i.e., the average absolute deviation between empirical and nominal coverage across confidence levels. These metrics have traditionally been used for uncertainty quantification in other contexts of machine learning [12, 16].

4 Results

Tables 1 and 2 collect all the evaluation metrics for models trained on heart rate-included inputs, acting as a performance summary for our work. In the Appendix, Tables 3 - 8 contain all other results pertaining to models trained on the three other classes of inputs. In this Section, we discuss various elements of model performance in terms of accuracy, the degree of calibration of the uncertainty quantification, and present several illustrative forecast diagrams to visualize how uncertainty estimates can be useful in glucose prediction.

4.1 On prediction and adverse glycemic event classification accuracy

In terms of the DTS Error Grid zone A accuracy, Transformer-based models, in particular those equipped with evidential output layers, achieved the best performance across experiments involving all four groups of input sequences and both horizon periods. For each experiment, all neural network models scored higher zone A accuracies than the ridge regression baseline. In the aspect of MARD, a specific model clearly stood out – Transformer-based model equipped with evidential regression output layers, hereafter referred to as Transformer Evidential Model (TEM). This uncertainty-aware model attained the lowest value consistently across all experiments and again, whereas ridge regression was the worst model in each case. The mean degradation of Zone A across all considered models at the longer horizon relative to the shorter horizon was about 8%, accompanied by an average increase in MARD of about 4%.

A critical aspect of glucose prediction system lies in forecasting of adverse glycemic events, in particular, hypoglycemia. In the aspect of sensitivity in detecting hypoglycemia, we found that evidential regression-equipped models and ridge regression yielded the highest values for both horizon lengths, with a sensitivity of ~ 0.9 for the longer horizon and about $\sim 5\%$ higher for the shorter one. As anticipated from precision-recall trade-off, evidential models scored lower in precision — a metric for which models unequipped with any uncertainty quantification methods performed the best. For hyperglycemia, the

relative capabilities among various model also displayed a similar trend, with evidential-based models scoring higher sensitivities yet lower precisions at both horizons compared to their counterparts.

At the level of per-patient metrics, we also investigated the sensitivity of our accuracy indices : the DTS zone A accuracy and MARD on the choice of input features, as we would like to know whether our results would reveal any particular choice of input features to be more discriminatory. Visual inspection of the population-level results in Tables 1 to 8 appears to show no significant dependence. We performed Friedman tests on the per-patient MARD and zone A accuracy scores attained by TEM across all four classes of inputs and for both horizon lengths. We found that apart from MARD results in the experiments involving 30 min horizon, there was no statistically significant effect ($p > 0.05$) of input features on these accuracy scores. For MARD values in the 30 min horizon setting, Friedman test revealed a statistically significant effect of input feature choice ($\chi^2(3) = 11.9, p < 0.01$), with heart rate-trained models being the best based on mean ranks. Effect size estimated using Kendall’s W was 0.16, indicating a small but consistent difference in ranking across patients. Post-hoc Wilcoxon signed-rank tests with Holm correction indicated heart rate-trained models to be better in MARD relative to those trained on steps and calories in the short horizon setting (Holm-adjusted $p \sim 0.01$), and better in ${}^{70}B$ score relative to that trained on steps in the long horizon setting (Holm-adjusted $p \sim 0.04$). For both types of accuracy metrics and horizon lengths, heart rate-trained models yielded the best mean scores. Based on these results, it thus appears that there is a slight advantage in model accuracy for heart rate-included inputs compared to the other three input classes defined by the inclusion of steps, calories and basal insulin. In the Appendix, Figures 6 and 7 show the boxplots for visualizing input feature dependence of per-patient accuracy metrics.

Table 1: Models trained on heart rate-included inputs (30 min horizon). Abbreviations: zA - zone A accuracy; MARD - mean absolute relative difference; ${}^{70}S$ - hypoglycemia sensitivity; ${}^{70}P$ - hypoglycemia precision; ${}^{70}B$ - hypoglycemia Brier score; ${}^{180}\{S, P, B\}$ - the corresponding metrics for hyperglycemia; MCE - mean calibration error; ρ - Spearman’s correlation between uncertainty and error; model subscripts d, e - equipped with Monte Carlo dropout and evidential regression respectively; ρ_z - Spearman’s correlation between uncertainty and clinical risk zones as defined in [18]. Each shaded cell pertains to the best-performing model for each metric column.

Model	zA	MARD	${}^{70}S$	${}^{70}P$	${}^{70}B$	${}^{180}S$	${}^{180}P$	${}^{180}B$	MCE	ρ	ρ_z
LSTM	96.7	4.52	0.80	0.95		0.91	0.97				
LSTM _d	96.6	4.66	0.88	0.81	0.018	0.92	0.94	0.023	0.10	0.15	0.073
LSTM _e	96.6	4.24	0.94	0.73	0.016	0.96	0.88	0.020	0.04	0.67	0.201
Transf	96.7	4.44	0.78	0.96		0.91	0.97				
Transf _d	96.8	4.50	0.87	0.84	0.018	0.93	0.94	0.022	0.09	0.23	0.098
Transf _e	96.8	4.14	0.94	0.73	0.015	0.96	0.87	0.019	0.03	0.68	0.208
GRU	96.7	4.49	0.77	0.97		0.91	0.96				
GRU _d	96.8	4.80	0.91	0.74	0.020	0.93	0.93	0.022	0.07	0.19	0.065
GRU _e	96.5	4.33	0.94	0.72	0.016	0.96	0.86	0.021	0.05	0.63	0.176
Ridge Reg.	95.5	5.69	0.94	0.61	0.021	0.96	0.79	0.026	0.12	0.48	0.203

Table 2: Models trained on heart rate-included inputs (60 min horizon).

Model	zA	MARD	${}^{70}S$	${}^{70}P$	${}^{70}B$	${}^{180}S$	${}^{180}P$	${}^{180}B$	MCE	ρ	ρ_z
LSTM	87.5	9.26	0.63	0.94		0.80	0.96				
LSTM _d	87.9	8.97	0.73	0.84	0.035	0.82	0.94	0.046	0.21	0.13	0.102
LSTM _e	88.8	8.32	0.88	0.63	0.027	0.90	0.81	0.038	0.02	0.68	0.327
Transf	88.7	8.62	0.63	0.95		0.80	0.97				
Transf _d	88.4	8.77	0.72	0.85	0.033	0.83	0.94	0.044	0.19	0.29	0.167
Transf _e	89.2	8.11	0.89	0.62	0.026	0.91	0.81	0.037	0.01	0.68	0.337
GRU	88.6	8.65	0.63	0.95		0.81	0.96				
GRU _d	88.1	8.94	0.76	0.77	0.034	0.84	0.93	0.043	0.14	0.13	0.075
GRU _e	88.8	8.26	0.88	0.62	0.027	0.90	0.81	0.038	0.02	0.66	0.336
Ridge Reg.	85.9	10.10	0.88	0.55	0.032	0.92	0.70	0.044	0.10	0.52	0.315

4.2 On the degree of calibration of uncertainty estimates

The metrics we use to measure the degree of calibration of the uncertainty estimates are: the Brier scores for hypoglycemia ${}^{70}B$ and hyperglycemic ${}^{180}B$ classifications of each predicted event, the mean calibration error (MCE) and the Spearman’s correlation coefficients ρ, ρ_z between uncertainty estimates and the prediction error and the DTS clinical risk zones. We found that TEM models were associated with the highest Spearman’s correlation of ~ 0.7 , with all evidential models yielding $\rho > 0.6$, generally at least twice higher than the corresponding dropout-based models. Ridge Regression models generally had $\rho \sim 0.5$. These results were consistently similar for both the horizon periods and all the four classes of input sequences the models were trained on. In the aspect of ρ_z , evidential models tended to have relatively higher scores of about ~ 0.3 for the long horizon and ~ 0.2 for the short horizon, indicating a non-trivial positive correlation between uncertainty estimates and the discrete DTS clinical risk zones. Ridge regression also performed comparably in this index with slightly lower values whereas dropout models yielded $\rho_z \sim 0.1$. Among all models, TEM models performed the best with an average (across different input classes) value of $\rho_z \sim 0.34$, showing that its uncertainty estimates were informative with respect to clinically defined risk zones, with higher uncertainties tending to correspond to predictions associated with greater clinical risk.

In the aspect of MCE, evidential models yielded the lowest values compared to dropout-based models and ridge regression. In particular, TEM models attained the best scores in each experiment. In Fig. 1, we plot the ECP vs NCP plots for three different models trained on the heart rate-included inputs with prediction horizon being 30 min. The ideal plot is characterized by the ECP curve being very close to the nominal straight line joining the origin to the point (1,1). As shown in Fig. 1, ridge regression’s calibration plot reveals an under-confident uncertainty distribution whereas Monte Carlo dropout (incorporated within a Transformer-based model) yielded an over-confident uncertainty distribution. When the same base model is equipped with an evidential output layer instead, the calibration plot shows an ECP curve that is very close to the ideal straight line, revealing a well-calibrated uncertainty quantification.

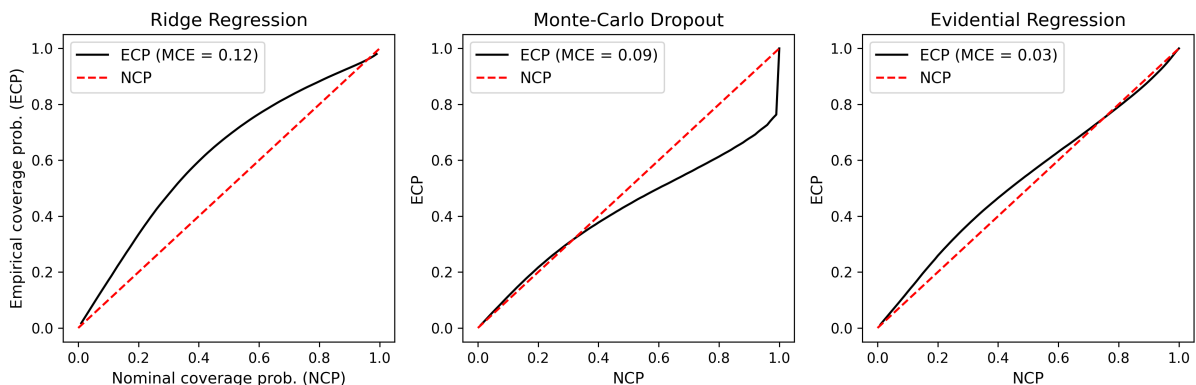


Fig. 1: Plot of empirical coverage probabilities (ECP) vs nominal coverage probabilities (NCP) for three types of models trained on heart rate-included inputs and defined by a 30 min prediction horizon. MCE denotes the mean calibration error which is the average of the absolute value of deviation between ECP and NCP.

In this aspect of Brier scores, evidential models yielded the lowest values for both hypoglycemia and hyperglycemia, with TEM models attaining the best scores in each experiment. Unlike MCE, there was degradation of Brier scores for the experiments involving the longer horizon with increments of about 0.01 for ${}^{70}B$ and of about 0.02 for ${}^{180}B$.

At the level of the distribution of per-patient-defined ${}^{70}B$ Brier score, for the optimal TEM models, we performed Friedman tests across all four sets of input features and for both choices of horizon durations. While we found no statistically significant effect ($p > 0.05$) of input features on ${}^{70}B$ in the short horizon setting, for the long horizon experiments, Friedman test revealed a statistically significant effect of input feature choice ($\chi^2(3) = 11.2, p \approx 0.01$), with heart rate-trained models being the best based on mean ranks. Effect size estimated using Kendall’s W was 0.15, indicating a small but consistent difference in ranking across patients. Conversely, at the level of the distribution of per-patient-defined ${}^{180}B$ Brier scores, we found no statistical significance for input feature dependence ($p > 0.05$ for both horizons). In

the Appendix, Fig. 8 and 9 show the boxplots for visualizing input feature dependence of per-patient-defined accuracy metrics.

4.3 Forecast Diagrams

To visualize the different implications of a strongly or weakly calibrated uncertainty quantification, we furnish a couple of representative rolling forecast plots. At each temporal point of measurement, we take the mean of all overlapping prediction windows which encompass the point, and similarly for the $\pm 2\sigma$ confidence bands surrounding it. Fig. 2a shows the full forecast plot for TEM model trained on basal insulin-included inputs with 1 hour horizon for a specific patient (labeled as ‘3’ in the HUPA-UCM dataset). The three dashed ellipses locate three examples of temporal regions where model would fail to detect hypoglycemia events unless uncertainty estimates are used. The 2σ uncertainty band is visibly larger at inflection points and its magnitude correlates with prediction errors. This is not always the case for a generic model.

Fig. 2b plots the rolling forecast for Transformer model equipped with Monte Carlo dropout trained on the same inputs and patient as Fig. 2a. We can see that there is a much weaker correlation between prediction errors and uncertainty estimates, with a number of regions where the uncertainty bands do not adequately cover the deviations between model predictions and the measured values. This is reflected in the relatively higher MCE, the over-confident empirical coverage probability plot (see Fig. 1) and the lower Spearman’s coefficient ρ between uncertainty estimates and errors. In this case, the uncertainty bands cannot be interpreted robustly and we have a poorly calibrated uncertainty quantification system.

In Figures 3 and 4, we furnish several illustrative plots showing single long horizon predictions for the TEM model, zooming onto a few points of Fig. 2a which are local neighborhoods of hypoglycemia and hyperglycemia events. These plots illustrate how uncertainty estimates can be useful for enhancing detection of hypo- and hyperglycemia events even when model predictions deviate from actual glucose trajectories, due to the coverage provided by the uncertainty bands. For example, in Fig. 3, within both prediction windows, the predicted glucose is deviating away from the threshold even while the actual measured glucose has crossed over, but the 1σ uncertainty interval encompasses the hypoglycemia region, and thus could have provided appropriate alert warnings if used in the prediction system.

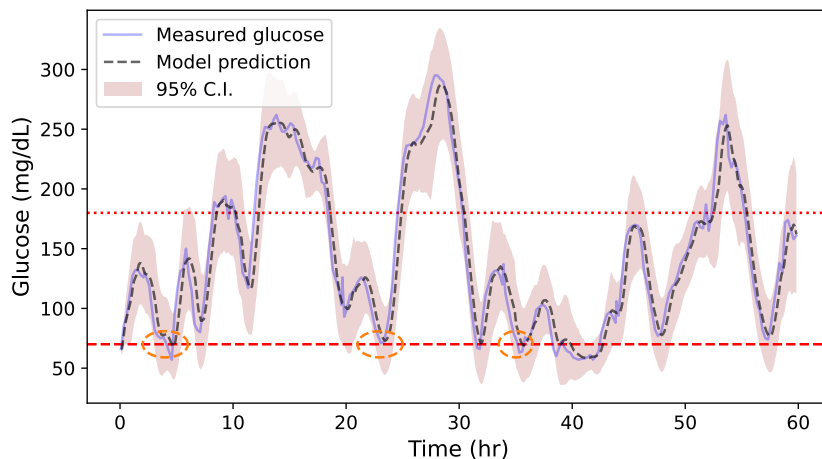
For uncertainty-aware models, we can increase sensitivity to adverse glycemic events by using the confidence intervals associated with the uncertainty distribution. The caveat is that the enhanced sensitivity led to a corresponding decrease in precision, and thus we have kept track of the Brier scores as a more holistic measure comparing among different models with respect to the detection of adverse glycemic events.

5 Discussion

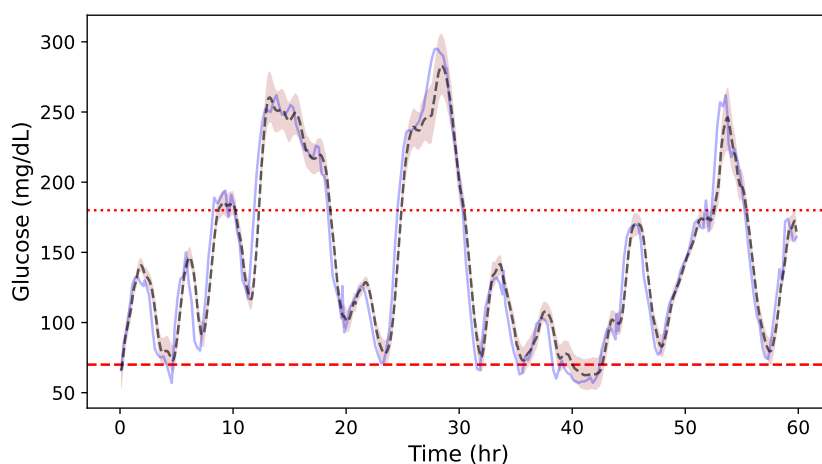
Our various experimental results indicated evidential regression-based models to be more effective in terms of uncertainty quantification than Monte Carlo dropout when both are applied across the three basic model structures : LSTM, GRU and Transformer-based architectures. This was characterized by lower Brier scores for adverse glycemic event identification, lower MCE and significantly higher Spearman’s coefficients between uncertainty and errors/clinical risk zones. The fact that this superiority held for all three base model types, all four classes of inputs and for both horizon durations suggests that it may be a fundamental strength of evidential regression-based uncertainty quantification over the more traditional dropout method in this application context. Ridge regression yielded higher Spearman’s coefficients than the dropout method, although its Brier scores in adverse glycemic event identification were not always higher/lower for all inputs, base model types and horizon lengths. In contrast to evidential regression-based models, dropout models did not display consistent superiority in various metrics over the baseline ridge regression.

In terms of the accuracy metrics, evidential models were consistently better than their dropout and ordinary (no uncertainty quantification) counterparts in the aspect of MARD for all input types and both horizon durations. For the longer horizon experiments, in the aspect of DTS zone A accuracy, evidential models were also consistently superior than their counterparts although this was not always the case for the shorter horizon experiments. Overall, these trends indicated that apart from equipping models with well-calibrated uncertainty quantification, evidential models were also superior in terms of accuracy defined via these clinically relevant metrics.

Within the family of evidential models trained on some specific input type and horizon period, we have identified the TEM model to be most effective in terms of MCE, ρ , ρ_z , the Brier scores for hypo-

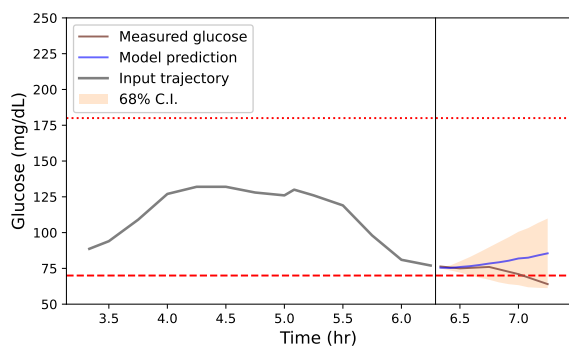


(a)

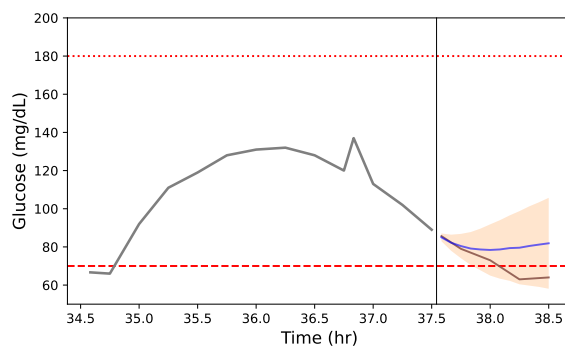


(b)

Fig. 2: The rolling forecast plot for TEM model (a) and Transformer-based model with Monte Carlo dropout (b) trained on basal insulin-included inputs with 1 hour horizon for Patient with ID ‘3’ in the HUPA dataset [14], with hypoglycemia (<math><70 \text{ mg/dL}</math>) and hyperglycemia (>math>>180 \text{ mg/dL}</math>) thresholds being represented by red, horizontal dashed lines. Dashed ellipses locate examples of regions where model would fail to detect hypoglycemia events unless uncertainty estimates are used.



(a)



(b)

Fig. 3: Single long horizon prediction windows for a couple of points near hypoglycemia thresholds in Fig. 2a, with the vertical lines in each diagram marking the start of the prediction horizon. In both prediction windows, the predicted glucose is deviating away from the threshold even when the actual measured glucose has crossed over, but the 1σ uncertainty interval encompasses the hypoglycemia region.

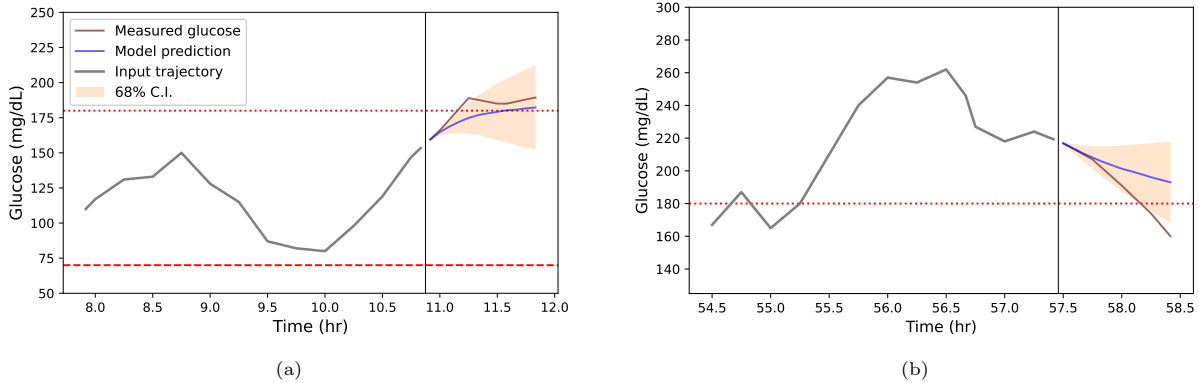


Fig. 4: Single long horizon prediction windows for a couple of points near hyperglycemia thresholds in Fig. 2a. In (a), the predicted glucose did not exceed the threshold even when the actual measured glucose has crossed over, but the 1σ uncertainty interval encompasses the hyperglycemia region. In (b), the predicted glucose level hovers above the threshold even when the actual measured value has dipped below it, but the size of the 1σ uncertainty interval appropriately captures the deviations.

and hyperglycemia event identification, relative to LSTM and GRU-based counterparts. In the aspect of accuracy, it yielded the lowest MARD in every case. For hypoglycemia sensitivity score and DTS zone A accuracy, it also yielded the best scores for most experimental settings (apart from those involving basal and steps-included inputs with 30 min horizon). Overall, these various results indicated that this particular model is a promising candidate for an uncertainty-aware glucose-prediction system, and can potentially complement more traditional hypoglycemia prediction techniques [26].

We have performed each experimental setting for two choices of horizon periods, and found the horizon-induced deterioration of accuracy to be roughly 4% for MARD and 8% for DTS zone A accuracy. For uncertainty quantification-related metrics, we found that while the Brier scores consistently deteriorated by about 0.01 for hypoglycemia and 0.02 for hyperglycemia, there was no significant and universal trend for MCE and ρ . The adverse glycemic event sensitivity metrics ${}^{70}S$, ${}^{180}S$ were also consistently lower for experiments with longer horizons compared to their shorter horizon counterparts. Conversely, ρ_z was consistently higher for experiments with longer horizons instead.

In this work, four families of 4-feature input sequences were considered, each consisting of blood glucose, carbohydrates ingested, bolus insulin and one of the following: heart rate, steps, calories and basal insulin. Results did not reveal any significant advantage that any input group has over others, although restricting to the most effective TEM model, at the level of the distribution of individual patient’s accuracy scores, heart rate-included inputs yielded a model that was slightly better in MARD (short horizon) and ${}^{70}B$ (long horizon).

Apart from numerical indices reflecting accuracy and degree of calibration of uncertainty estimates, calibration diagrams showed that for evidential models, the empirical coverage probabilities were much closer to nominal ones relative to other models, with Monte Carlo dropout’s uncertainty quantification being over-confident and that of ridge regression being under-confident. The forecast diagrams in Figures 2, 3, 4 depicted how the confidence bands could enhance sensitivity to adverse glycemic events, in particular, hypoglycemia detection. We have also computed the Brier scores to assess the probabilistic classification more holistically. These metrics and associated visual aids appeared to indicate that evidential models were well-calibrated in their uncertainty estimates.

6 Limitations and Ethical Considerations

6.1 Limitations

We would like to point out a couple of natural future directions of our work here.

1. We have used population-level (all 25 patients of the HUPA dataset [14]) training data in all our experiments. It would be interesting to carry out similar investigations using individual patient’s data instead to probe the feasibility and relative effectiveness of a more personalized glucose prediction model. In [23], the HUPA-UCM dataset was also studied and the authors reported that models trained on individual patients appeared to have similar prediction accuracy as those trained at a

population level. In theory, population-level models would capture trends universal across diabetic patients whereas patient-specific models only learn intra-patient variability.

2. There are many other input feature combinations for which we can perform a comparative study. Here, we have kept to four-feature inputs similar to [23], with glucose, bolus insulin and carbohydrates being included in all four classes of inputs examined. It would be worthwhile to consider more extensive permutations of input variables to see if there are synergistic combinations.

6.2 Ethical considerations

Our work here used the publicly available HUPA-UCM dataset [14], which consists of de-identified patient data collected with informed consent. No personally identifiable information was accessed. According to [14], this dataset was approved by the ethical committee of Hospital Universitario Príncipe de Asturias de Madrid, and all 25 patients had signed an informed consent form. (Protocol Number: EC/11/2018, Date of approval: December 12th 2018. [14]) We also emphasize that while the models developed in this work aim to support glucose forecasting, they are not intended for autonomous clinical decision-making.

7 Conclusion

In this work, we have examined a number of uncertainty-aware neural network models for blood glucose prediction and adverse glycemic event identification relevant for Type 1 diabetes management. With the base models being one of the three families of sequence models defined by LSTM, GRU, and Transformer architectures, uncertainty quantification was implemented by either Monte Carlo dropout or through evidential output layers compatible with Deep Evidential Regression. Using the HUPA-UCM diabetes dataset of [14] for validation, we identified Transformer-based models equipped with evidential outputs to furnish the most effective uncertainty-aware framework, achieving consistently higher predictive accuracies as measured by MARD and DTS error grid zone A accuracy, as well as better-calibrated uncertainty estimates whose magnitudes significantly correlated with prediction errors and clinical risk zones. This class of models deserves further study as a promising candidate for an uncertainty-aware glucose prediction system that can complement traditional adverse glycemic event prediction techniques. Overall, our work has shown that incorporating uncertainty quantification through evidential regression can lead to robust glucose prediction models that are not merely accurate, but also rigorously informative with regards to its inherent predictive confidence.

Acknowledgments

I am grateful to Rafe McBeth for various discussions and past collaborations [28–30] on related topics involving uncertainty quantification in machine learning. This work was initiated during TAAI 2025 where a related study involving evidential regression and Bergman’s model for diabetes pathophysiology was presented [30]. I thank the conference organizers for providing an inspiring environment.

A Appendix

A.1 On DTS error grids

In Fig. 5, we display a couple of DTS error grid diagrams for two particular patients with relatively larger differences in their risk zone distributions. The model predictions for Patient ‘1’ of [14] are characterized by a larger spread in risk zone levels in contrast to those for Patient ‘9’ of [14]. The DTS error grid diagrams can be used as a visual aid in assessing model reliability which is lower for Patient ‘1’ relative to Patient ‘9’.

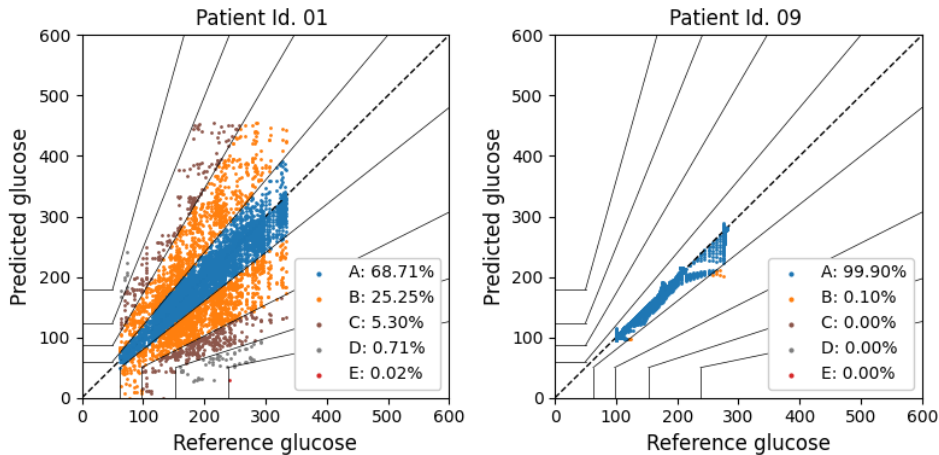


Fig. 5: DTS error grids for two patients with marked difference in their risk zone distributions. The various pairs of solid lines defined away from the dashed diagonal mark the boundaries of the five risk zones.

A.2 An information-theoretic regularization loss term in evidential regression

With regards to our regularizer loss term \mathcal{L}_{kl} , we had obtained it by taking the KL divergence between the normal-inverse-gamma (NIG) distribution parametrized by $\{\gamma, \alpha, \beta, \nu\}$ and another reference NIG distribution with $\{\gamma_r, \alpha_r, \beta_r, \nu_r\}$ that presumably characterizes a non-/weakly informative prior. When multiplied to a term such as $|y_{obs} - \gamma|$ in eqn. (7), it implies that for more significantly large errors, the loss term guides the distributions for such samples to approach a weakly-informative one yielding higher uncertainty. By definition, the KL divergence between two NIG distributions with density functions (\tilde{p}_r, \tilde{p}) is

$$D_{KL}(\tilde{p}_r || \tilde{p}) = \iint d\bar{u} d\sigma_u^2 \tilde{p}_r \log \frac{\tilde{p}_r}{\tilde{p}}, \quad (8)$$

where u denotes the target variable (glucose level in our context) assumed to follow a normal distribution with mean \bar{u} and variance σ_u^2 . As a prior for this assumed normal distribution, the NIG distribution can be equivalently understood as the product

$$\bar{u} \sim \mathcal{N}\left(\gamma, \frac{\sigma_u^2}{\nu}\right), \quad \sigma_u^2 \sim \Gamma^{-1}(\alpha, \beta).$$

We would like the reference prior to be a non- or weakly-informative prior. Taking the limit of $\nu_r \rightarrow \infty$ yields a uniform distribution over \mathbb{R} which is unfortunately unnormalizable. To avoid this pathology, we take the reference NIG to be parametrized by values of γ, ν identical to those of the evidential model outputs’ distributions, and instead set the reference inverse-gamma distribution to be of relatively higher entropy, taking $\alpha_r = 1$ and letting β_r be task-dependent. Since the variance σ_u^2 is not physically expected to be larger than the upper bound for u , a natural candidate for β_r is the maximal glucose value in our training dataset. This definition of \tilde{p}_r leads to the KL divergence term being

$$\mathcal{D}_{KL} = \left(\log \frac{\beta_r^\alpha \Gamma(\alpha)}{\beta^\alpha} + \gamma_e(\alpha - 1) + \frac{\beta - \beta_r}{\beta_r} \right). \quad (9)$$

Further, like in [2], we consider using a simple linear term $|y_{obs} - \gamma|$ that aims to increase the loss for predictions with larger errors, and multiply it to the KL term in eqn. (9) to obtain our final expression for the regularizer loss term

$$\mathcal{L}_{kl} = |y_{obs} - \gamma| D_{kl}. \quad (10)$$

A.3 Boxplots for visualizing input feature dependence of per-patient-defined metrics

Figures 6, 7, 8 and 9 display the boxplots for various per-patient-metrics: MARD, zone A accuracy, ^{70}B and ^{180}B Brier scores respectively. These accuracy score distributions are those of the TEM model which, at the population level, attained the best accuracy and uncertainty calibration scores. To quantify the degree of sensitivity to the choice of input features, we performed Friedman tests across all four sets of input features and for both choices of horizon durations. There are only two statistically significant ($p < 0.01$) cases: MARD (short horizon) and ^{70}B Brier score (long horizon). For MARD values in the 30 min horizon setting, Friedman test revealed a statistically significant effect of input feature choice with statistic $\chi^2(3) = 11.9$ ($p < 0.01$), whereas for ^{70}B in the long horizon setting, the Friedman statistic reads $\chi^2(3) = 11.2$ ($p \approx 0.01$). Post-hoc Wilcoxon signed-rank tests with Holm correction indicated heart rate-trained models with short prediction horizon to achieve better MARD than those trained on steps and calories (Holm-adjusted $p \sim 0.01$), and heart rate-trained models with long prediction horizon achieving higher ^{70}B scores than those trained on steps (Holm-adjusted $p \sim 0.04$).

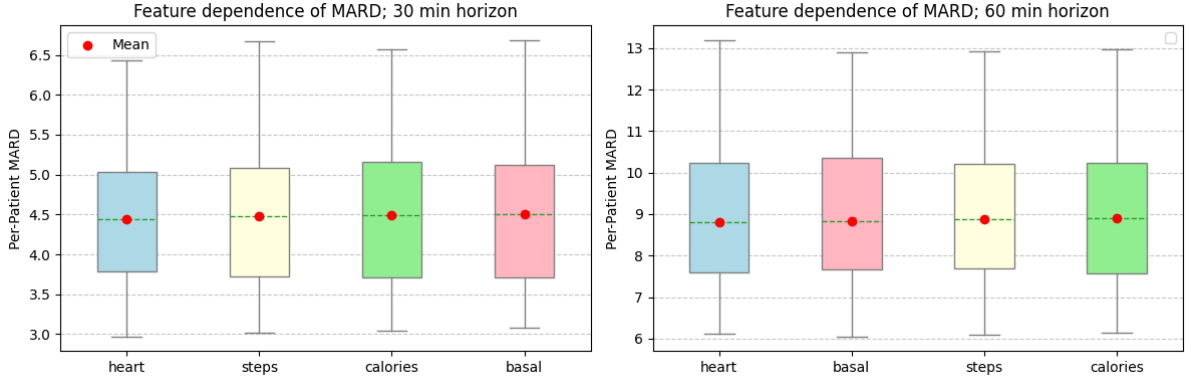


Fig. 6: Boxplots showing the distribution of per patient MARD values for each class of input features. Friedman test was significant ($p < 0.01$) for the short horizon setting, with post-hoc Wilcoxon signed-rank tests with Holm correction indicating heart rate-trained models to achieve better MARD than those trained on steps and calories (Holm-adjusted $p \sim 0.01$).

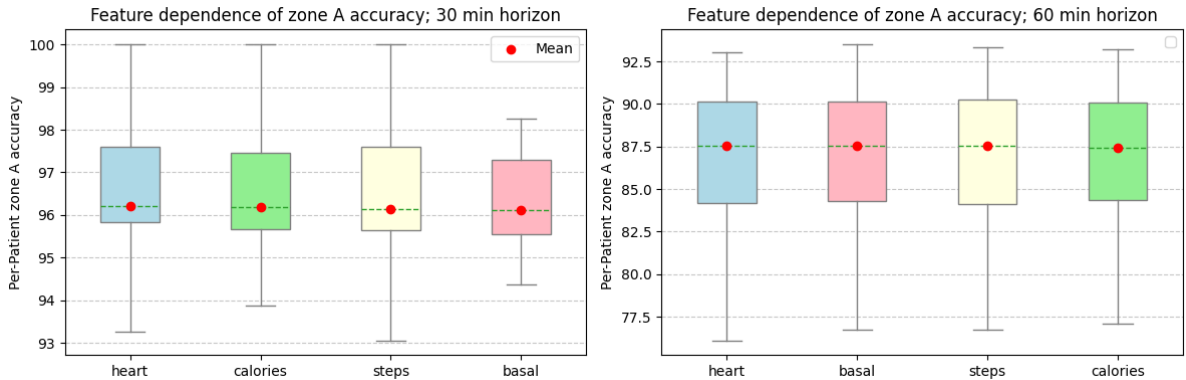


Fig. 7: Boxplots showing the distribution of per patient DTS zone A accuracy for each class of input features. Friedman test indicated no statistically significant difference among various models.

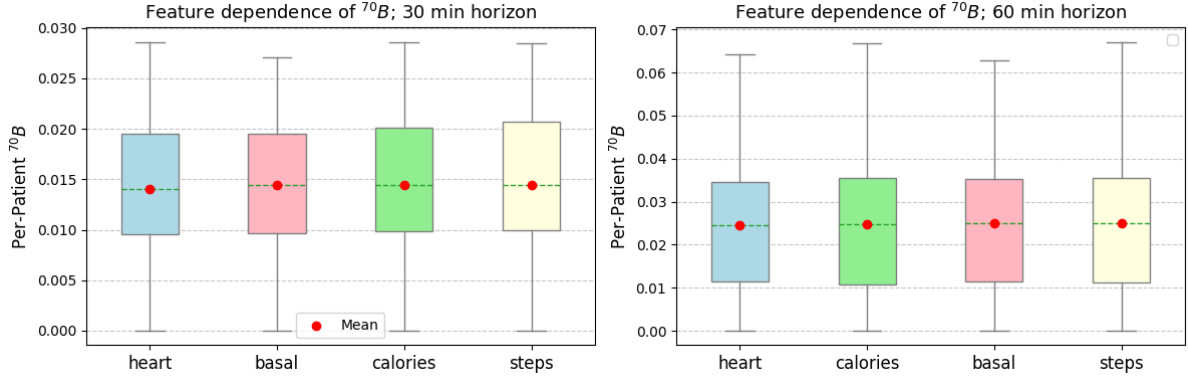


Fig. 8: Boxplots showing the distribution of per patient ^{70}B values for each class of input features. Friedman test was significant ($p \sim 0.01$) for the long horizon setting, with post-hoc Wilcoxon signed-rank tests with Holm correction indicating heart rate-trained models to achieve higher ^{70}B than those trained on steps (Holm-adjusted $p \sim 0.04$)

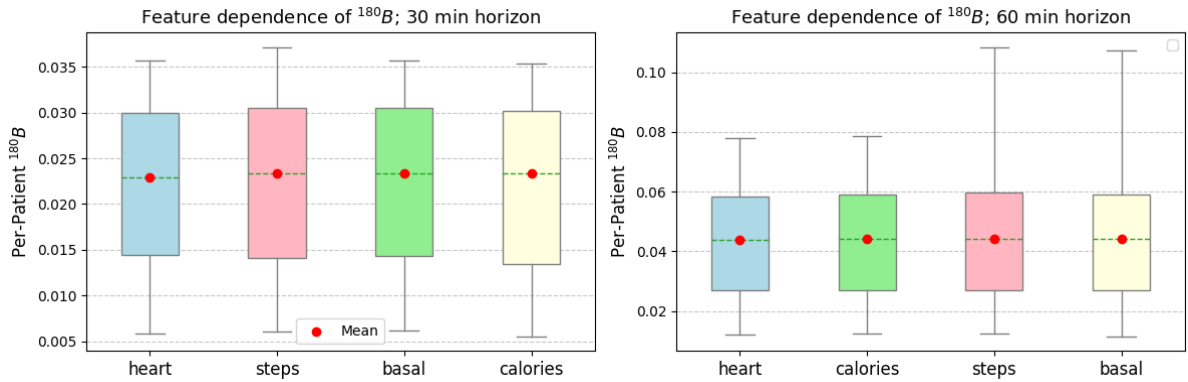


Fig. 9: Boxplots showing the distribution of per patient DTS ^{180}B values for each class of input features. Friedman test indicated no statistically significant difference among various models.

A.4 Other experimental results

We have performed experiments based on four input features : glucose, bolus insulin, carbohydrates and one of the following { heart rate, steps, calories and basal insulin }. In the main text, Tables 1 and 2 collect various results for heart rate-based inputs. In this Appendix, Tables 3 - 8 collect various results for models trained on basal insulin, calories and steps-included inputs.

Table 3: Models trained on basal insulin-included inputs (30 min horizon). Abbreviations: zA - zone A accuracy; MARD - mean absolute relative difference; ${}^{70}S$ - hypoglycemia sensitivity; ${}^{70}P$ - hypoglycemia precision; ${}^{70}B$ - hypoglycemia Brier score; ${}^{180}\{S, P, B\}$ - the corresponding metrics for hyperglycemia; MCE - mean calibration error; ρ - Spearman’s correlation between uncertainty and error; model subscripts d, e - equipped with Monte Carlo dropout and evidential regression respectively; ρ_z - Spearman’s correlation between uncertainty and clinical risk zones as defined in [18]. Each shaded cell pertains to the best-performing model for each metric column.

Model	zA	MARD	${}^{70}S$	${}^{70}P$	${}^{70}B$	${}^{180}S$	${}^{180}P$	${}^{180}B$	MCE	ρ	ρ_z
LSTM	96.7	4.46	0.79	0.95		0.90	0.97				
LSTM _d	96.6	4.64	0.88	0.82	0.018	0.92	0.94	0.023	0.10	0.16	0.071
LSTM _e	96.6	4.26	0.94	0.73	0.016	0.96	0.88	0.020	0.04	0.68	0.192
Transf	96.9	4.36	0.79	0.95		0.90	0.97				
Transf _d	96.7	4.53	0.86	0.84	0.018	0.93	0.94	0.022	0.08	0.25	0.097
Transf _e	96.8	4.20	0.94	0.72	0.015	0.96	0.87	0.020	0.02	0.68	0.205
GRU	96.8	4.38	0.78	0.96		0.91	0.97				
GRU _d	96.6	4.77	0.91	0.73	0.020	0.93	0.93	0.022	0.07	0.20	0.062
GRU _e	96.5	4.29	0.94	0.72	0.016	0.96	0.87	0.020	0.05	0.65	0.203
Ridge	95.5	5.67	0.95	0.60	0.021	0.96	0.79	0.026	0.12	0.48	0.199

Table 4: Models trained on basal insulin-included inputs (60 min horizon).

Model	zA	MARD	${}^{70}S$	${}^{70}P$	${}^{70}B$	${}^{180}S$	${}^{180}P$	${}^{180}B$	MCE	ρ	ρ_z
LSTM	87.9	8.96	0.63	0.94		0.80	0.96				
LSTM _d	88.0	8.92	0.73	0.84	0.035	0.82	0.94	0.046	0.22	0.14	0.100
LSTM _e	88.7	8.33	0.88	0.63	0.028	0.90	0.82	0.038	0.02	0.67	0.322
Transf	88.5	8.63	0.62	0.96		0.80	0.97				
Transf _d	88.4	8.70	0.72	0.86	0.033	0.83	0.94	0.044	0.20	0.27	0.180
Transf _e	89.2	8.14	0.90	0.61	0.027	0.90	0.82	0.037	0.004	0.68	0.334
GRU	88.3	8.71	0.62	0.96		0.80	0.97				
GRU _d	87.9	9.00	0.75	0.80	0.034	0.84	0.92	0.043	0.15	0.16	0.063
GRU _e	88.8	8.31	0.88	0.62	0.027	0.90	0.82	0.038	0.01	0.66	0.327
Ridge	85.9	10.06	0.89	0.54	0.033	0.92	0.70	0.044	0.10	0.52	0.314

Table 5: Models trained on steps-included inputs (30 min horizon).

Model	zA	MARD	${}^{70}S$	${}^{70}P$	${}^{70}B$	${}^{180}S$	${}^{180}P$	${}^{180}B$	MCE	ρ	ρ_z
LSTM	96.7	4.48	0.80	0.95		0.90	0.97				
LSTM _d	96.6	4.64	0.88	0.82	0.018	0.92	0.94	0.023	0.10	0.15	0.074
LSTM _e	96.6	4.24	0.94	0.73	0.016	0.96	0.88	0.020	0.040	0.68	0.196
Transf	96.9	4.38	0.79	0.95		0.90	0.97				
Transf _d	96.7	4.52	0.87	0.84	0.018	0.93	0.94	0.022	0.091	0.24	0.103
Transf _e	96.8	4.18	0.94	0.72	0.015	0.96	0.87	0.020	0.020	0.67	0.208
GRU	96.8	4.39	0.78	0.96		0.91	0.97				
GRU _d	96.6	4.69	0.91	0.74	0.020	0.93	0.93	0.022	0.07	0.18	0.058
GRU _e	96.5	4.30	0.94	0.74	0.016	0.96	0.87	0.020	0.042	0.66	0.208
Ridge	95.5	5.66	0.95	0.61	0.021	0.96	0.80	0.026	0.12	0.48	0.202

Table 6: Models trained on steps-included inputs (60 min horizon).

Model	zA	MARD	${}^{70}S$	${}^{70}P$	${}^{70}B$	${}^{180}S$	${}^{180}P$	${}^{180}B$	MCE	ρ	ρ_z
LSTM	87.6	9.17	0.63	0.95		0.80	0.95				
LSTM _d	88.1	8.92	0.73	0.84	0.034	0.82	0.94	0.046	0.21	0.14	0.096
LSTM _e	88.8	8.31	0.88	0.63	0.028	0.90	0.81	0.038	0.02	0.67	0.326
Transf	88.6	8.63	0.62	0.95		0.80	0.96				
Transf _d	88.5	8.70	0.71	0.85	0.033	0.83	0.94	0.044	0.20	0.31	0.180
Transf _e	89.3	8.12	0.89	0.61	0.026	0.90	0.82	0.037	0.007	0.68	0.338
GRU	88.6	8.60	0.62	0.96		0.80	0.97				
GRU _d	88.2	8.90	0.76	0.79	0.033	0.83	0.93	0.043	0.14	0.16	0.078
GRU _e	88.8	8.28	0.87	0.63	0.027	0.90	0.80	0.038	0.02	0.65	0.336
Ridge	86.0	10.03	0.89	0.54	0.033	0.92	0.70	0.044	0.10	0.52	0.316

Table 7: Models trained on calories-included inputs (30 min horizon).

Model	zA	MARD	${}^{70}S$	${}^{70}P$	${}^{70}B$	${}^{180}S$	${}^{180}P$	${}^{180}B$	MCE	ρ	ρ_z
LSTM	96.7	4.58	0.79	0.95		0.90	0.97				
LSTM _d	96.4	5.04	0.87	0.83	0.019	0.91	0.94	0.025	0.147	0.15	0.072
LSTM _e	96.6	4.26	0.94	0.74	0.016	0.96	0.87	0.020	0.043	0.67	0.194
Transf	96.5	4.76	0.78	0.96		0.90	0.97				
Transf _d	96.4	4.85	0.87	0.84	0.019	0.92	0.94	0.024	0.12	0.24	0.101
Transf _e	96.9	4.19	0.94	0.72	0.015	0.96	0.88	0.020	0.015	0.68	0.205
GRU	96.8	4.39	0.79	0.96		0.90	0.97				
GRU _d	96.7	4.77	0.91	0.74	0.020	0.92	0.95	0.022	0.069	0.16	0.056
GRU _e	96.5	4.33	0.93	0.74	0.016	0.96	0.87	0.020	0.034	0.63	0.189
Ridge Reg.	95.6	5.65	0.95	0.61	0.021	0.96	0.80	0.025	0.121	0.47	0.201

Table 8: Models trained on calories-included inputs (60 min horizon).

Model	zA	MARD	${}^{70}S$	${}^{70}P$	${}^{70}B$	${}^{180}S$	${}^{180}P$	${}^{180}B$	MCE	ρ	ρ_z
LSTM	87.9	9.08	0.62	0.96		0.80	0.97				
LSTM _d	87.7	9.18	0.72	0.84	0.035	0.81	0.94	0.047	0.232	0.122	0.092
LSTM _e	88.8	8.33	0.88	0.64	0.028	0.90	0.82	0.038	0.013	0.673	0.322
Transf	88.6	8.70	0.64	0.94		0.80	0.97				
Transf _d	88.2	8.88	0.71	0.85	0.034	0.83	0.94	0.045	0.206	0.302	0.181
Transf _e	89.1	8.17	0.88	0.64	0.026	0.90	0.81	0.037	0.014	0.682	0.338
GRU	88.5	8.65	0.62	0.97		0.80	0.97				
GRU _d	88.0	9.00	0.76	0.79	0.033	0.84	0.93	0.043	0.147	0.133	0.080
GRU _e	88.7	8.38	0.88	0.62	0.028	0.90	0.81	0.038	0.018	0.650	0.331
Ridge Reg.	86.0	10.03	0.89	0.54	0.032	0.92	0.70	0.044	0.099	0.515	0.316

References

1. American Diabetes Association Professional Practice, C.: 6. glycemic goals and hypoglycemia: Standards of care in diabetes-2024. *Diabetes Care* **47**(Suppl 1), S111–S125 (Jan 2024)
2. Amini, A., Schwarting, W., Soleimany, A., Rus, D.: Deep evidential regression. In: Proceedings of the 34th International Conference on Neural Information Processing Systems. NIPS '20, Curran Associates Inc., Red Hook, NY, USA (2020)
3. Battelino, T., Alexander, C.M., Amiel, S.A., Arreaza-Rubin, G., Beck, R.W., Bergenstal, R.M., Buckingham, B.A., Carroll, J., Ceriello, A., Chow, E., Choudhary, P., Close, K., Danne, T., Dutta, S., Gabbay, R., Garg, S., Heverly, J., Hirsch, I.B., Kader, T., Kenney, J., Kovatchev, B., Laffel, L., Maahs, D., Mathieu, C., Mauricio, D., Nimri, R., Nishimura, R., Scharf, M., Del Prato, S., Renard, E., Rosenstock, J., Saboo, B., Ueki, K., Umpierrez, G.E., Weinzimer, S.A., Phillip, M.: Continuous glucose monitoring and metrics for clinical trials: an international consensus statement. *Lancet Diabetes Endocrinol* **11**(1), 42–57 (Jan 2023)
4. Battelino, T., Danne, T., Bergenstal, R.M., Amiel, S.A., Beck, R., Biester, T., Bosi, E., Buckingham, B.A., Cefalu, W.T., Close, K.L., Cobelli, C., Dassau, E., DeVries, J.H., Donaghue, K.C., Dovc, K., Doyle, F.J.r., Garg, S., Grunberger, G., Heller, S., Heinemann, L., Hirsch, I.B., Hovorka, R., Jia, W., Kordonouri, O., Kovatchev, B., Kowalski, A., Laffel, L., Levine, B., Mayorov, A., Mathieu, C., Murphy, H.R., Nimri, R., Nørgaard, K., Parkin, C.G., Renard, E., Rodbard, D., Saboo, B., Schatz, D., Stoner, K., Urakami, T., Weinzimer, S.A., Phillip, M.: Clinical targets for continuous glucose monitoring data interpretation: Recommendations from the international consensus on time in range. *Diabetes Care* **42**(8), 1593–1603 (Aug 2019)
5. Brier, G.: Verification of forecasts expressed in terms of probability, 'monthly weather review', 78 (1) (1950)
6. Cho, K., van Merriënboer, B., Gülçehre, Ç., Bougares, F., Schwenk, H., Bengio, Y.: Learning phrase representations using RNN encoder-decoder for statistical machine translation. *CoRR* **abs/1406.1078** (2014), <http://arxiv.org/abs/1406.1078>
7. Cinar, B., van den Boom, L., Maleshkova, M.: Review of machine learning models in short- and long-term glucose forecasting and hypoglycemia classification. *Informatics in Medicine Unlocked* **60**, 101723 (2026)
8. Clarke, W.L., Cox, D., Gonder-Frederick, L.A., Carter, W., Pohl, S.L.: Evaluating clinical accuracy of systems for self-monitoring of blood glucose. *Diabetes Care* **10**(5), 622–628 (09 1987)
9. Cover, T.M., Thomas, J.A.: Elements of Information Theory (Wiley Series in Telecommunications and Signal Processing). Wiley-Interscience, USA (2006)
10. Danne, T., Nimri, R., Battelino, T., Bergenstal, R.M., Close, K.L., DeVries, J.H., Garg, S., Heinemann, L., Hirsch, I., Amiel, S.A., Beck, R., Bosi, E., Buckingham, B., Cobelli, C., Dassau, E., Doyle, F.J.r., Heller, S., Hovorka, R., Jia, W., Jones, T., Kordonouri, O., Kovatchev, B., Kowalski, A., Laffel, L., Maahs, D., Murphy, H.R., Nørgaard, K., Parkin, C.G., Renard, E., Saboo, B., Scharf, M., Tamborlane, W.V., Weinzimer, S.A., Phillip, M.: International consensus on use of continuous glucose monitoring. *Diabetes Care* **40**(12), 1631–1640 (Dec 2017)
11. Gal, Y., Ghahramani, Z.: Dropout as a bayesian approximation: Representing model uncertainty in deep learning. In: Balcan, M.F., Weinberger, K.Q. (eds.) Proceedings of The 33rd International Conference on Machine Learning. Proceedings of Machine Learning Research, vol. 48, pp. 1050–1059. PMLR, New York, New York, USA (20–22 Jun 2016), <https://proceedings.mlr.press/v48/gal16.html>
12. Gneiting, T., Raftery, A.E.: Strictly proper scoring rules, prediction, and estimation. *Journal of the American Statistical Association* **102**(477), 359–378 (03 2007)
13. Gregg, E.W., Sattar, N., Ali, M.K.: The changing face of diabetes complications. *Lancet Diabetes Endocrinol* **4**(6), 537–547 (Jun 2016)
14. Hidalgo, J.I., Alvarado, J., Botella, M., Aramendi, A., Velasco, J.M., Garnica, O.: Hupa-ucm diabetes dataset. *Data in Brief* **55**, 110559 (2024)
15. Hochreiter, S., Schmidhuber, J.: Long short-term memory. *Neural Comput* **9**(8), 1735–1780 (Nov 1997)
16. Jungo, A., Reyes, M.: Assessing reliability and challenges of uncertainty estimations for medical image segmentation (2019)
17. Kendall, A., Gal, Y.: What uncertainties do we need in bayesian deep learning for computer vision? In: Proceedings of the 31st International Conference on Neural Information Processing Systems. p. 5580–5590. NIPS'17, Curran Associates Inc., Red Hook, NY, USA (2017)
18. Klonoff, D.C., Freckmann, G., Pleus, S., Kovatchev, B.P., Kerr, D., Tse, C.C., Li, C., Agus, M.S.D., Dungan, K., VoglováHagerf, B., Krouwer, J.S., Lee, W.A.A., Misra, S., Rhee, S.Y., Sabharwal, A., Seley, J.J., Shah, V.N., Tran, N.K., Waki, K., Worth, C., Tian, T., Aaron, R.E., Rutledge, K., Ho, C.N., Ayers, A.T., Adler, A., Ahn, D.T., Aktürk, H.K., Al-Sofiani, M.E., Bailey, T.S., Baker, M., Bally, L., Bannuru, R.R., Bauer, E.M., Bee, Y.M., Blanchette, J.E., Cengiz, E., Chase, J.G., Y Chen, K., Cherrāvsky, D., Clements, M., Cote, G.L., Dhatariya, K.K., Drincic, A., Ejksjaer, N., Espinoza, J., Fabris, C., Fleming, G.A., Gabbay, M.A.L., Galindo, R.J., Gómez-Medina, A.M., Heinemann, L., Hermanns, N., Hoang, T., Hussain, S., Jacobs, P.G., Jendle, J., Joshi, S.R., Koliwad, S.K., Lal, R.A., Leiter, L.A., Lind, M., Mader, J.K., Maran, A., Masharani, U., Mathioudakis, N., McShane, M., Mehta, C., Moon, S.J., Nichols, J.H., O'Neal, D.N., Pasquel, F.J., Peters, A.L., Pfützner, A., Pop-Busui, R., Ranjitkar, P., Rhee, C.M., Sacks, D.B., Schmidt, S., Schwaighofer, S.M., Sheng, B., Simonson, G.D., Sode, K., Spanakis, E.K., Spartano, N.L., Umpierrez, G.E., Vareth, M., Vesper, H.W., Wang, J., Wright, E., Wu, A.H.B., Yeshiwas, S., Zilbermint, M., Kohn, M.A.: The diabetes technology

- society error grid and trend accuracy matrix for glucose monitors. *J Diabetes Sci Technol* **18**(6), 1346–1361 (Nov 2024)
19. Kullback, S., Leibler, R.A.: On Information and Sufficiency. *The Annals of Mathematical Statistics* **22**(1), 79 – 86 (1951)
 20. Langarica, S., de la Vega, D., Cariman, N., Miranda, M., Andrade, D.C., Nunez, F., Rodriguez-Fernandez, M.: Deep learning-based glucose prediction models: A guide for practitioners and a curated dataset for improved diabetes management. *IEEE Open J Eng Med Biol* **5**, 467–475 (2024)
 21. Liu, K., Li, L., Ma, Y., Jiang, J., Liu, Z., Ye, Z., Liu, S., Pu, C., Chen, C., Wan, Y.: Machine learning models for blood glucose level prediction in patients with diabetes mellitus: Systematic review and network meta-analysis. *JMIR Med Inform* **11**, e47833 (Nov 2023)
 22. MacKay, D.J.C.: Bayesian interpolation. *Neural Computation* **4**(3), 415–447 (05 1992)
 23. Manchanda, E., Zeng, J., Lo, C.H.: Data-efficiency with comparable accuracy: Personalized lstm neural network training for blood glucose prediction in type 1 diabetes management. *Diabetology* **6**(10) (2025)
 24. Marling, C., Bunescu, R.: The ohiot1dm dataset for blood glucose level prediction: Update 2020. *CEUR Workshop Proc* **2675**, 71–74 (Sep 2020)
 25. Rama Chandran, S., Rahman, N., Gandhi, M., Tan, N.C., Phoon, I.K.Y., Seah, D.E.J., Cheah, M.H., Sek, K., Gardner, D.S.L.: Intermittently scanned continuous glucose monitoring provides no benefit over structured self-monitoring of blood glucose in type 2 diabetes not on prandial insulin, in the context of diabetes self-management education: Glucose monitoring programme singapore (glimpse). *Diabetes Res Clin Pract* **211**, 111678 (May 2024)
 26. Rama Chandran, S., Tay, W.L., Lye, W.K., Lim, L.L., Ratnasingam, J., Tan, A.T.B., Gardner, D.S.L.: Beyond hba1c: Comparing glycemic variability and glycemic indices in predicting hypoglycemia in type 1 and type 2 diabetes. *Diabetes Technol Ther* **20**(5), 353–362 (May 2018)
 27. Sensoy, M., Kaplan, L., Kandemir, M.: Evidential deep learning to quantify classification uncertainty (2018), <https://arxiv.org/abs/1806.01768>
 28. Tan, H.S., Wang, K., McBeth, R.: Deep evidential learning for radiotherapy dose prediction. *Computers in Biology and Medicine* **182**, 109172 (Nov 2024). <https://doi.org/10.1016/j.compbimed.2024.109172>, <http://dx.doi.org/10.1016/j.compbimed.2024.109172>
 29. Tan, H.S., Wang, K., McBeth, R.: Evidential physics-informed neural networks (2025), <https://arxiv.org/abs/2501.15908>, presented at the SCML 2025 Conference
 30. Tan, H.S., Wang, K., McBeth, R.: Evidential physics-informed neural networks for scientific discovery. In: *Proceedings of the 30th International Conference on Technologies and Applications of Artificial Intelligence (TAAI)* (2025), <https://arxiv.org/abs/2509.14568>, also available as arXiv:2509.14568
 31. Tena, F., Garnica, O., Lanchares, J., Hidalgo, J.I.: An lstm-based neural network wearable system for blood glucose prediction in people with diabetes. *IEEE J Biomed Health Inform* **29**(8), 5515–5526 (Aug 2025)
 32. Vaswani, A., Shazeer, N., Parmar, N., Uszkoreit, J., Jones, L., Gomez, A.N., Kaiser, L., Polosukhin, I.: Attention is all you need (2023), <https://arxiv.org/abs/1706.03762>
 33. Zhu, T., Li, K., Herrero, P., Georgiou, P.: Personalized blood glucose prediction for type 1 diabetes using evidential deep learning and meta-learning. *IEEE Trans Biomed Eng* **70**(1), 193–204 (Jan 2023)